IEEE Open Journal of the
Industrial Electronics Society

Received 9 February 2023; revised 24 March 2023 and 21 April 2023; accepted 28 April 2023. Date of publication 1 May 2023;
date of current version 12 May 2023. The review of this article was arranged by Associate Editor Jingang Lai.

Digital Object Identifier 10.1109/OJIES.2023.3272030

Effective Circuit Configuration and Control for Coil-Array Wireless Power Transmitters

HIROKAZU MATSUMOTO (Member, IEEE), WATARU YONEYAMA, AOZORA HATA, AND YUKI SATO (Member, IEEE)

Aoyama Gakuin University, Sagamihara 252-5258, Japan

CORRESPONDING AUTHOR: HIROKAZU MATSUMOTO.(e-mail: Hmatsumoto@aoyamagakuin.jp).

ABSTRACT This article presents a circuit configuration and control for coil-array wireless power transmitters. The target coil arrays have coils that are uniform in shape and dimensions and are regularly arranged with an angular interval of 120°. The system has a three-leg half-bridge inverter, which simultaneously feeds the three coils in the transmitter. It can deal with more than three coils by adding a switch set between the inverter and the coils. The system has a configuration to cancel mutual inductances between the transmitter coils and improve the power factor of the system. It can maximize the efficiency from the transmitter coils to the receiver coil and can output uniform power regardless of the receiver position. The current condition for achieving these features is derived, and a field-programmable-gate-array-based control for realizing the current condition is presented. The performance of the proposed system is experimentally validated with an implemented prototype. Results show that the system has a power variation of less than 5.8% depending on the receiver position. The system can operate at approximately maximum efficiency.

INDEX TERMS Coil array, FPGA-based control, multileg inverter, optimal current control, three-phase system, wireless power transfer.

I. INTRODUCTION

When discussing wireless power transfer technology, misalignments between a transmitter and a receiver are inevitable issues. One of the approaches to the issue is the employment of a coil-array structure for the transmitter. The coil array arranged along a pathway gives one-dimensional freedom to the receiver. This array can be applied to a charger for moving vehicles [1], [2]. Coil array expanded on a plane gives two-dimensional freedom to the receiver, without exact position control of the receiver [3], [4], [5], [6], [7].

There are several circuit configurations to feed the coil-array transmitters [8]. An inverter simultaneously energizes multiple serial coils via a series resonant capacitor [9] or multiple parallel coils via an *LC* and *LCL* compensator [10], [11]. These configurations can be fabricated simply and cost-effectively. On the other hand, the same number of inverters [12], [13] as that of the coils or a half-bridge inverter [14], [15], [16], [17], [18] with the same number of legs can be used. Only the transmitter coils close to the received coil are energized by the inverter, which leads to high-efficiency and low-magnetic-leakage operation. In recent years, configurations where the switches are set between the inverter and the transmitter coils have been researched [19]. The switch selects the transmitter coils close to the receiver to connect the coils with the inverter. The switch can be a low-speed-switching device, such as electromagnetic relays, which is more cost-effective than switching devices used in the inverters. Thus, the configurations can be realized in low cost and can be operated in high efficiency and in low magnetic leakage. However, the following issues have not been addressed yet.

1) The power assignment of the transmitter coils is not optimized. For instance, a current is uniformly drawn into all the active coils regardless of the magnetic coupling with the receiver coil. This operation is inefficient because the coils away from the receiver do not contribute to the power transfer while the coils generate loss. To gain higher transfer efficiency, the currents through the transmitter coils should be allocated appropriately.
2) Uniform power transfer is not always ensured with respect to the receiver position. A multilayer coil-array

transmitter [3], [20] is a structure capable of uniform power transfer. However, it is not suitable for high-power applications. In the coil-array transmitters formed on a layer, the magnetic coupling with the receiver varies considerably with respect to the receiver position. Therefore, for example, the receiver above the clearance between the transmitter coils and the receiver just above a transmitter coil have different powers unless the currents through the coils are not controlled appropriately.

3) Mutual inductance between the transmitter coils is not considered or is disregarded. The mutual inductance as well as the self-inductance of the coils degrade the power factor of the system. They should be canceled to improve performance.

This article proposes an effective circuit configuration and a control method for coil-array wireless power transmitters. The proposed configuration and control can be applied to the coil-array transmitter with considerably variable magnetic coupling with the receiver. In this article, the target transmitter is a coil array formed on a layer. The system comprises a three-leg half-bridge inverter, which simultaneously feeds three coils in the transmitter. The system can deal with numerous coils by adding a switch set between the inverter and the coils in the system. The system can cancel the mutual inductances between the transmitter coils with the additional resonant reactance element that is set between the connection of the transmitter coils and the inverter. The system can control the currents through the transmitter coils so that the efficiency between the transmitter coils and the receiver coil is maximized and the transfer power is uniform regardless of the receiver position. Unlike [21], [22], and [23], the control can achieve this performance with the voltage and current information in the inverter and without knowing the values of the mutual inductance between the transmitter and the receiver and the receiver position. Therefore, the proposed control can operate dynamically.

The rest of this article is organized as follows. Section II describes the circuit configuration and parameters of the resonant reactance element. Section III derives the optimal current through the coils, and Section IV validates the performance of the optimal current control numerically. Section V presents the implementation of the field-programmable gate array (FPGA)-based control. In addition, the pulse-width modulation algorithm to eliminate the influence of dead time is presented. Section VI experimentally examines the proposed system with an implemented prototype and validates its performance. Finally, Section VII concludes this article.

II. PROPOSED CIRCUIT CONFIGURATION

A. CIRCUIT CONFIGURATION

Fig. 1 shows a concept of target coil-array transmitters, where the three coils L_u, L_v, and L_w with the same structure and the same dimensions are regularly arranged with an interval of 120°. In addition to the coils forming a hexagonal shape [3],

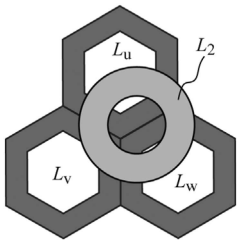

FIGURE 1. Coil-array transmitter with three coils and a receiver coil.

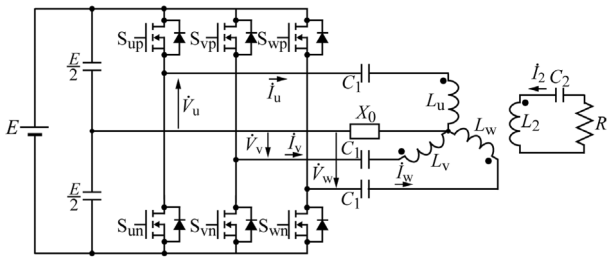

FIGURE 2. Proposed circuit configuration for the coil-array transmitter with three coils.

[20], the proposed circuit configuration and control can also be applied to circular-shaped and square-shaped coils. The receiver coil L_2 is set over the array via a vertical air gap l_g in length. The arrangement of the transmitter coils does not ensure a uniform power transfer, even if current uniformly flows through the coils.

Fig. 2 shows the proposed circuit configuration for a coil array with three coils. The three-leg half-bridge inverter feeds the coil array. Each coil is connected to a leg of the inverter via the capacitor C_1. Another end of the coil is y-connected with the others, and the connection is led to the inverter via the resonant reactance element X_0. In the figure, although the connection leads to a potential of $E/2$ in the inverter, any potential between zero and E can be applied to it.

Because of the symmetrical structure of the coil-array transmitter, the self-inductances and the resistances of the coils and the mutual inductances between the coils can be represented by L_1, r_1, and M_1 respectively. The equivalent equation of the transmitter is given as follows:

$$\begin{aligned}\begin{bmatrix}\dot{V}_u\\ \dot{V}_v\\ \dot{V}_w\end{bmatrix} &= r_1\begin{bmatrix}\dot{I}_u\\ \dot{I}_v\\ \dot{I}_w\end{bmatrix} + j\omega L_1\begin{bmatrix}\dot{I}_u\\ \dot{I}_v\\ \dot{I}_w\end{bmatrix} + \frac{1}{j\omega C_1}\begin{bmatrix}\dot{I}_u\\ \dot{I}_v\\ \dot{I}_w\end{bmatrix}\\ &\quad + j\omega\begin{bmatrix}0 & M_1 & M_1\\ M_1 & 0 & M_1\\ M_1 & M_1 & 0\end{bmatrix}\begin{bmatrix}\dot{I}_u\\ \dot{I}_v\\ \dot{I}_w\end{bmatrix} + j\omega\begin{bmatrix}M_{u2}\\ M_{v2}\\ M_{w2}\end{bmatrix}\dot{I}_2\\ &\quad + jX_0\begin{bmatrix}1 & 1 & 1\\ 1 & 1 & 1\\ 1 & 1 & 1\end{bmatrix}\begin{bmatrix}\dot{I}_u\\ \dot{I}_v\\ \dot{I}_w\end{bmatrix}\end{aligned} \tag{1}$$

where $\dot{V}_u$, $\dot{V}_v$, and $\dot{V}_w$ are the output phase voltages of the inverter, and $\dot{I}_u$, $\dot{I}_v$, and $\dot{I}_w$ are the currents through the

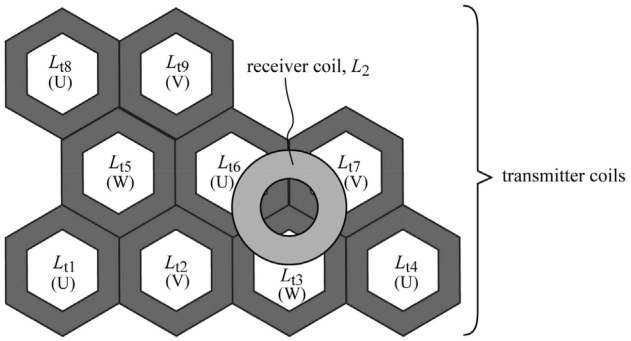

FIGURE 3. Expanded coil-array transmitter and receiver coil.

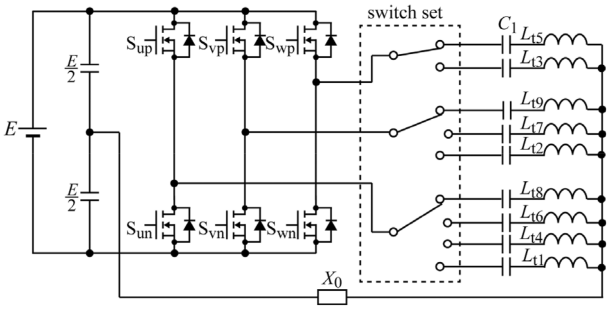

FIGURE 4. Circuit configuration for the expanded coil-array transmitter.

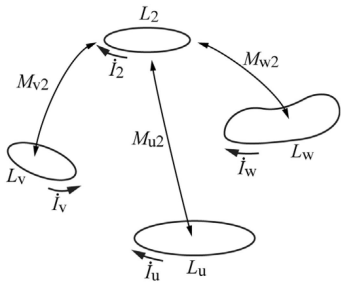

FIGURE 5. Arbitrarily arranged three transmitter coils and receiver coil.

transmitter coils. M_{u2}, M_{v2}, and M_{w2} denote the mutual inductances between the transmitter coils and the receiver coil. Arranging this equation yields the following:

$$\begin{bmatrix} \dot{V}_u \\ \dot{V}_v \\ \dot{V}_w \end{bmatrix} = r_1 \begin{bmatrix} \dot{I}_u \\ \dot{I}_v \\ \dot{I}_w \end{bmatrix} + j\omega (L_1 - M_1) \begin{bmatrix} \dot{I}_u \\ \dot{I}_v \\ \dot{I}_w \end{bmatrix} + \frac{1}{j\omega C_1} \begin{bmatrix} \dot{I}_u \\ \dot{I}_v \\ \dot{I}_w \end{bmatrix} + j (X_0 + \omega M_1) \begin{bmatrix} 1 & 1 & 1 \\ 1 & 1 & 1 \\ 1 & 1 & 1 \end{bmatrix} \begin{bmatrix} \dot{I}_u \\ \dot{I}_v \\ \dot{I}_w \end{bmatrix} + j\omega \begin{bmatrix} M_{u2} \\ M_{v2} \\ M_{w2} \end{bmatrix} \dot{I}_2. \tag{2}$$

Setting the capacitor C_1 and the reactance value X_0 at

$$C_1 = \frac{1}{\omega^2 (L_1 - M_1)} \tag{3a}$$

$$X_0 = -\omega M_1 \tag{3b}$$

yields

$$\begin{bmatrix} \dot{V}_u \\ \dot{V}_v \\ \dot{V}_w \end{bmatrix} = r_1 \begin{bmatrix} \dot{I}_u \\ \dot{I}_v \\ \dot{I}_w \end{bmatrix} + j\omega \begin{bmatrix} M_{u2} \\ M_{v2} \\ M_{w2} \end{bmatrix} \dot{I}_2. \tag{4}$$

Thus, the reactance in the transmitter can be completely canceled. In the coil-array transmitter shown in Fig. 1, the mutual inductance M_1 has a negative value, and an inductor L_0 with the following inductance is used as X_0:

$$L_0 = |M_1|. \tag{5}$$

Alternatively, when the coils in the transmitter are widely overlapped with each other, M_1 can have a positive value. In this case, a capacitor C_0 with the following capacitance is used as X_0:

$$C_0 = \frac{1}{\omega^2 M_1}. \tag{6}$$

B. EXPANDED CIRCUIT CONFIGURATION

Fig. 3 shows an expanded coil-array transmitter. Fig. 4 shows the circuit configuration for the expanded coil-array transmitter. The transmitter circuit has a configuration where a switch set is added to the circuit shown in Fig. 2. The circuit can be fabricated with less switches than that presented in [19], although the magnetic coupling with the receiver varies larger, which leads to ununiform power transfer unless the proposed configuration and control are not employed. In the circuit, a resonant capacitor is set on every coil. If the self-inductances of the coils in a group are the same, a capacitor can be set in every group. Three groups, U, V, and W are assigned to the coils and the legs in the inverter. The switch set connects an inverter leg to the coil that belongs to the same group as the leg and is the closest to the receiver coil in the group. For example, when the receiver coil is set at the position shown in Fig. 3, the U-leg, V-leg, and W-leg are connected with L_{t6}, L_{t7}, and L_{t3}, respectively. As a result, any combinations of active three coils have a positional relation with the receiver coil, like the relation shown in Fig. 1, where L_u, L_v, and L_w are the coils of the U-group, V-group, and W-group, respectively. This article is focused on the efficient power transfer in the coil-array transmitter with three coils, and the switchover of the coils is outside the scope of this article.

III. CONTROL ALGORITHM

The optimal current maximizing the efficiency between the transmitter coils and the receiver coil is derived in this section. The first discussion is for the case where three coils are different in shape and dimensions and are arbitrarily arranged in three-dimensional space, as shown in Fig. 5. In this case, the coils have different resistances, r_u, r_v, and r_w. The circuit configuration shown in Fig. 2 is used to feed the wireless power transfer coils. The receiver coil has the self-inductance

L_2 and the resistance r_2. C_2 completely resonates with L_2. The load is assumed to be a resistor R for simplification.

The output power P_R and resistive losses P_{r1} and P_{r2} in the transmitter and the receiver are given as follows:

$$P_{r1} = r_u|\dot{I}_u|^2 + r_v|\dot{I}_v|^2 + r_w|\dot{I}_w|^2 \tag{7a}$$

$$P_{r2} = r_2\left(\frac{|\dot{V}_{2i}|}{R + r_2}\right)^2 \tag{7b}$$

$$P_R = R\left(\frac{|\dot{V}_{2i}|}{R + r_2}\right)^2 \tag{7c}$$

where $\omega = 2\pi f$ is the operation angular frequency of the system, and $\dot{V}_{2i}$ is the induced voltage in the receiver coil. The voltage is given as follows:

$$\dot{V}_{2i} = j\omega\begin{bmatrix}\dot{I}_u & \dot{I}_v & \dot{I}_w\end{bmatrix}\begin{bmatrix}M_{u2}\\ M_{v2}\\ M_{w2}\end{bmatrix}. \tag{8}$$

The transfer efficiency η_c between the transmitter coils and the receiver coil is defined as follows:

$$\eta_c = \frac{P_R}{P_{r1} + P_{r2} + P_R}. \tag{9}$$

Equations (7) and (9) imply that the maximum efficiency is available when P_{r1} is minimized under a fixed voltage $|\dot{V}_{2i}|$. The current condition required to satisfy this can be obtained by solving the geometric question that asks the tangent point of a plane represented by (8) and an ellipsoid represented by (7a) in the rectangular coordinate system with I_u, I_v, and I_w. At the tangent point, the directions of the normal vectors of the two geometries correspond to each other. Therefore, the optimal currents are given as follows:

$$\begin{bmatrix}I_u\\ I_v\\ I_w\end{bmatrix} = \lambda\begin{bmatrix}M_{u2}/r_u\\ M_{v2}/r_v\\ M_{w2}/r_w\end{bmatrix} \tag{10}$$

where λ is a coefficient. Because the mutual inductances are in proportion to the induced voltages V_{ui}, V_{vi}, and V_{wi} in the transmitter coils:

$$\begin{bmatrix}\dot{V}_{ui}\\ \dot{V}_{vi}\\ \dot{V}_{wi}\end{bmatrix} = j\omega\begin{bmatrix}M_{u2}\\ M_{v2}\\ M_{w2}\end{bmatrix}\dot{I}_2 \tag{11}$$

equation (10) can be changed to

$$\begin{bmatrix}I_u\\ I_v\\ I_w\end{bmatrix} = \lambda'\begin{bmatrix}V_{ui}/r_u\\ V_{vi}/r_v\\ V_{wi}/r_w\end{bmatrix}. \tag{12}$$

Thus, optimal currents are available with these induced voltages and the resistances of the coils. Based on (4) with the perfectly resonant receiver, the induced voltages can be calculated with

$$\begin{bmatrix}V_{ui}\\ V_{vi}\\ V_{wi}\end{bmatrix} = \begin{bmatrix}V_u\\ V_v\\ V_w\end{bmatrix} - \begin{bmatrix}r_uI_u\\ r_vI_v\\ r_wI_w\end{bmatrix}. \tag{13}$$

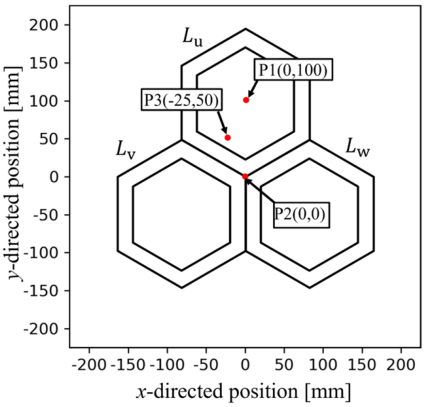

FIGURE 6. Schematic diagram of the coil-array transmitter.

Consequently, on the basis of (12), the current command values I_{uc}, I_{vc}, and I_{wc} for the optimal current control are defined by the following equation:

$$\begin{bmatrix}I_{uc}\\ I_{vc}\\ I_{wc}\end{bmatrix} = \frac{P_{2c}}{\frac{V_{ui}^2}{r_u} + \frac{V_{vi}^2}{r_v} + \frac{V_{wi}^2}{r_w}}\begin{bmatrix}V_{ui}/r_u\\ V_{vi}/r_v\\ V_{wi}/r_w\end{bmatrix} \tag{14}$$

where P_{2c} is a power command value. The phase angle of the currents is set at 0 or π. When the induced voltage has a positive value, the phase angle is set to 0, otherwise, the phase angle is set to π. Controlling the currents at I_{uc}, I_{vc}, and I_{wc} can achieve uniform power transfer regardless of the receiver position. This is proved by substituting (14) into (8), which yields the following:

$$V_{2i} = \frac{P_{2c}}{\frac{V_{ui}^2}{r_u} + \frac{V_{vi}^2}{r_v} + \frac{V_{wi}^2}{r_w}}\left(\frac{V_{ui}M_{u2}}{r_u} + \frac{V_{vi}M_{v2}}{r_v} + \frac{V_{wi}M_{w2}}{r_w}\right). \tag{15}$$

Multiplying I_2 to both sides of the aforementioned equation and then arranging it yields the following:

$$P_{2c} = V_{2i}I_2. \tag{16}$$

Thus, the power $V_{2i}I_2$, which implies a power transferred to the receiver, corresponds to a constant, P_{2c}. Since the power $V_{2i}I_2$ is the sum of the output power P_R and the resistive loss in the receiver coil, P_R is given as follows:

$$P_R = \frac{R}{R + r_2}P_{2c}. \tag{17}$$

When the load resistance R is a constant, P_R is also a constant under a constant P_{2c}. When r_2 is much smaller than the load resistance R, P_{2c} can be assumed to be equal to P_R, that is, the system is robust over the fluctuation of the load resistance.

IV. NUMERICAL ANALYSIS

Fig. 6 shows a coil-array transmitter used to test the performance of the proposed system. The three coils, L_u, L_v, and L_w, with a hexagonal shape, are tightly arranged with

TABLE 1. Parameters for Analysis

L_1	40.28 μH	L_2	73.50 μH
r_1	90.1 mΩ	r_2	127.2 mΩ
f	85 kHz	l_g	50 mm

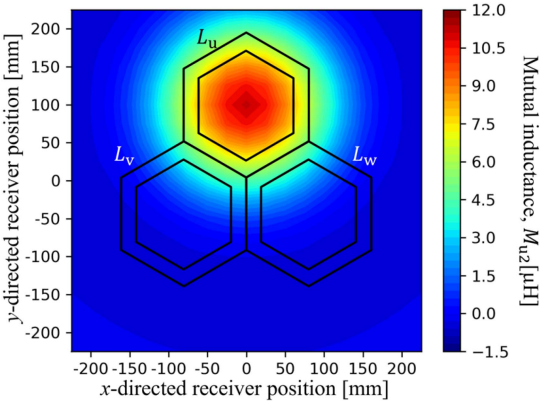

FIGURE 7. Mutual inductance between L_u and the receiver coil at receiver positions.

an interval of 120°. They have the same structure and the same dimensions. In [3] and [20], coil-array transmitters with hexagonal coils are implemented on multilayers of a printed circuit board. The arrangement with positional shifts every layer contributes to the uniform power transfer when a current is uniformly drawn to the coils. Alternatively, the array shown in Fig. 6 consists of windings made of wires on a layer. The one-layer structure is employed for the system dealing with a larger power [15]. Its drawback is that uniform power transfer is not ensured even if a current is uniformly drawn to the coils. The receiver coil has a circular shape and is set above the transmitter via an air gap. In the figure, the three positional points are defined; remarkably, P1 is the center of L_u and P2 is the contact point of the three coils. These points are used as representatives of the center positions of the receiver coil.

Table 1 lists the parameters used in the analysis. Because the transmitter coils have the same structure and the same dimensions, their resistances and self-inductances can be represented by r_1 and L_1, respectively.

Fig. 7 shows the mutual inductance M_{u2} between L_u and the receiver coil at receiver positions. These were calculated with finite-element analysis. The mutual inductances M_{v2} and M_{w2} of L_v and L_w with the receiver coil are distributed in the same manner.

Fig. 8 shows the distribution of resistance values that maximize transfer efficiency at receiver positions. The equilateral triangle in the figure has corners at the centers of the transmitter coils. In the expanded system shown in Figs. 3 and 4, when the receiver coil is outside the triangle, another combination of transmitter coils is used. Inside the triangle, the variation of the resistance is slight; 7.14 Ω is marked as a peak at P1, whereas 5.70 Ω is marked as a valley at P3. The average over the inside of the triangle is 5.81 Ω.

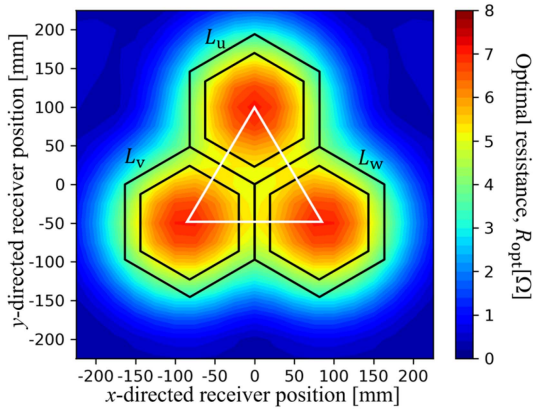

FIGURE 8. Optimal load resistance values at receiver positions.

Fig. 9 shows the power transfer efficiency η_c under $P_R = 500$ W and optimal load resistances at transmitter coil currents. As aforementioned, the currents distribute on a plane when the power is fixed at a level. To be exact, there is another plane capable of transferring the same power, which is arranged in point symmetry with the origin. In the symmetrical plane, the signs of the currents are inverse to the plane shown in these figures. It is confirmed that the optimal current command values calculated by (14) mark maximum efficiency.

Fig. 10 shows the variation of the optimal current command value I_u for L_u at receiver positions. Currents over 1.0 A distribute widely above parts of L_v and L_w. This implies that simultaneous energization of the three coils is necessary to improve the efficiency, especially around the contact edge of the coils. As a result, even at P2, an efficiency of 94.9% is available, as shown in Fig. 11. Fig. 12 shows the transfer efficiencies when a current is uniformly drawn to the three coils. In comparison with the optimal current condition, the area with efficiencies of more than 80% is smaller, and the peak value is lower by 1.5%. Thus, the proposed control using optimal currents has higher efficiencies than the conventional method.

V. IMPLEMENTATION OF CONTROL

A. CONTROL BLOCK DIAGRAMS

Fig. 13 shows the control block diagrams. The sensed current i_u through L_u is transformed to the real and imaginary components I_{u_re} and I_{u_im} of the fundamental with the discrete Fourier transform (DFT). The currents are controlled to a command value I_{uc} and zero, respectively, using proportional–integral (PI) control. I_{u_im} is zero without the control when the reactance of the coil array is completely canceled. The control can compensate for the deviation of the current phase owing to the existence of a slight reactance. The outputs of the PI control blocks are transformed into voltage with the phase angle θ_u and the magnitude V_u. Through similar control blocks, the voltages V_v and V_w for L_v and L_w are calculated to control i_v and i_w, respectively. The amplitudes of these voltages are used to generate current command values with (13) and (14). When the receiver coil is absent or away from

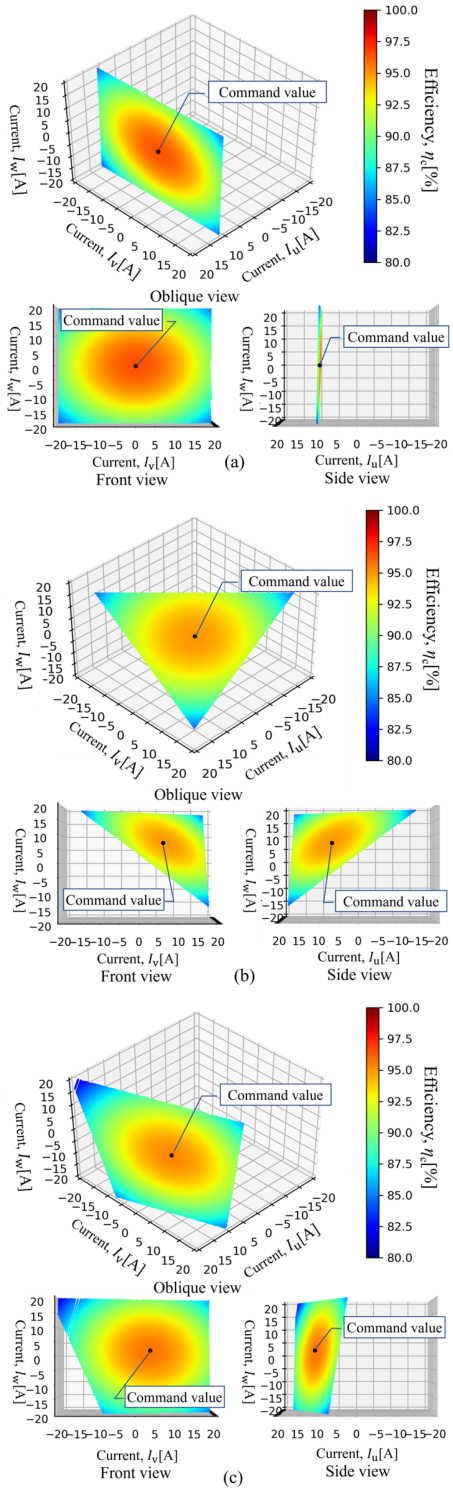

FIGURE 9. Efficiencies at currents when the receiver is at (a) P1, (b) P2, and (c) P3.

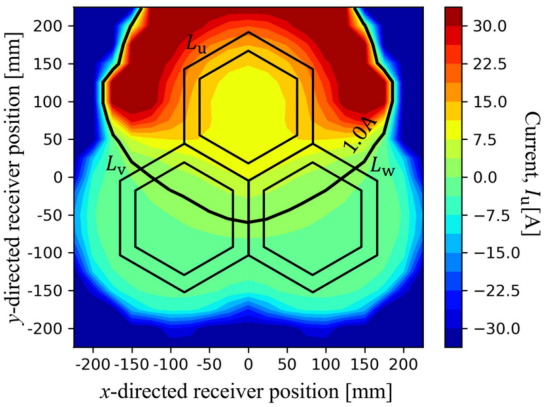

FIGURE 10. Optimal current command value I_u to transfer 500 W under a load resistance of 5.81 Ω at receiver positions.

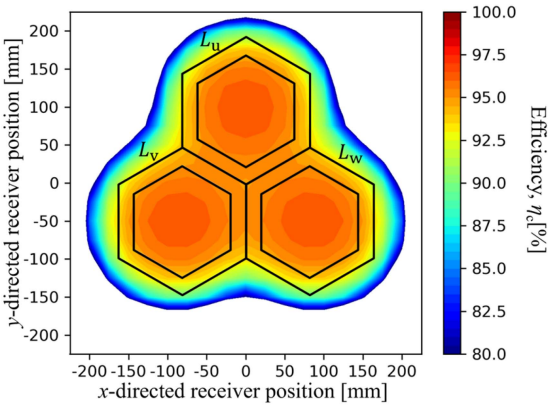

FIGURE 11. Transfer efficiencies, applying the optimal currents, under an output power of 500 W and a load resistance of 5.81 Ω at receiver positions.

Alternatively, the voltages V_u, V_v, and V_w are inputted to the one pulse modulation block, which generates switching signals for the inverter. Unlike one of the techniques described in [24], the one pulse modulation block has a function for compensating for dead time. Fig. 14 explains the algorithm for it. The signal S_{op} in Fig. 14(a) is an output of the conventional one pulse modulation block. The signals S_{up} and S_{un} turn ON with a lag of dead time t_d behind the switching of S_{op}. Since the output current in the inverter varies sinusoidally as shown in Fig. 14 owing to the resonant circuit, the output voltage is $-E/2$, during the dead time. As a result, the output voltage differs from the desired voltage. In the proposed method, turn-ON of S_{op} is advanced, and the turn-ON duration is expanded by t_d. It should be noted that the turn-ON duration is limited to half of the operation period. Consequently, the output voltage can have a desired width, as shown in Fig. 14(b).

the transmitter coils, the sum of squared induced voltages is significantly small. In this condition, the controller sets the current command values at a low level instead of (14), which can prevent overcurrent and allow the controller to detect the proximity of the receiver coil.

B. FPGA IMPLEMENTATION

The control was implemented in XILINX FPGA, XC7K160T-1FBG484C. The system clock is set at 87.04 MHz, which is 1024 times the fundamental operation frequency of 85 kHz. The currents are sensed and A/D converted every 16 clocks.

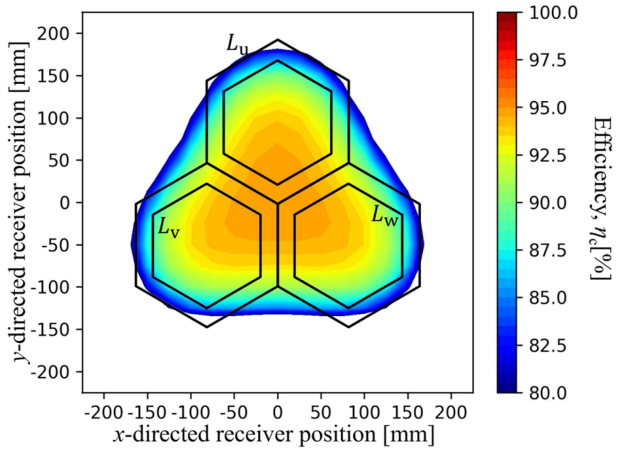

FIGURE 12. Transfer efficiencies, applying a current through the three coils under an output power of 500 W and a load resistance of 5.81 Ω at receiver positions.

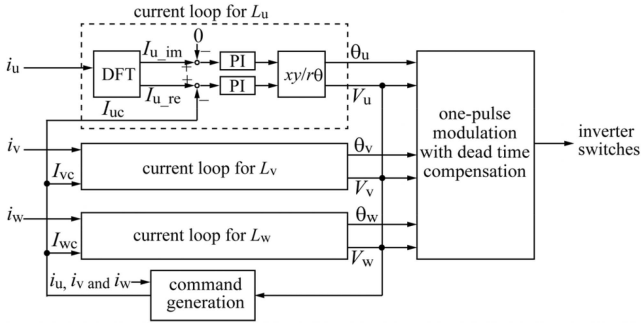

FIGURE 13. Control block diagrams.

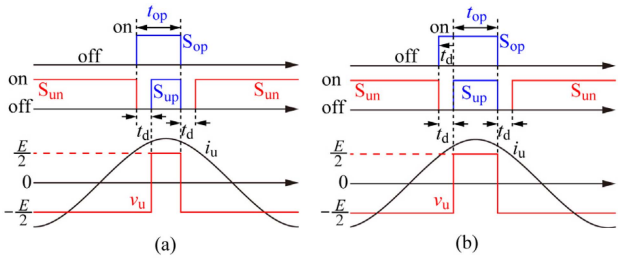

FIGURE 14. Switching signal, voltage, and current waveforms (a) without dead time compensation and (b) with dead time compensation.

Therefore, 64 digital data points are available per one cycle period of the fundamental. For DFT, 128 data points are used. The PI controls are executed every 4096 clock cycle. The command generation is executed every 65 536 clock cycle.

VI. EXPERIMENTS

A. EXPERIMENTAL CONDITIONS

Fig. 15 shows the experimental setup. Its system configuration is shown in Fig. 2, where the load consists of a rectifier and a resister R. The parameters of the system are listed in Table 2. The load resistor R is set to 8.85 Ω, which is calculated as the average value over the area inside of the triangle shown in Fig. 8, based on the measured parameters. This value is

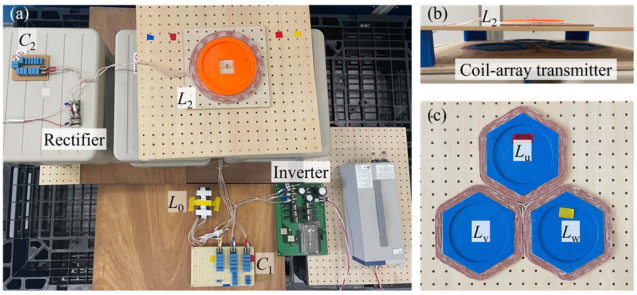

FIGURE 15. Experimental setup. (a) Top view of whole the system. (b) Side view of the coils. (c) Coil-array transmitter.

TABLE 2. Parameters of the System

E	150 V	f	85 kHz
number of turns L_u, L_v, L_w	12	number of turns L_2	16
L_u	43.31 μH	r_u	90.0 mΩ
L_v	43.15 μH	r_v	90.0 mΩ
L_w	42.95 μH	r_w	90.3 mΩ
L_2	80.26 μH	r_2	127.2 mΩ
M_{uv}	−2.90 μH	M_{uw}	−2.92 μH
M_{wu}	−2.80 μH	R	8.85 Ω

TABLE 3. Reactance Values of the Compensated Transmitter

X_u	1 mΩ	X_v	-25 mΩ	X_w	6 mΩ
X_{uv}	51 mΩ	X_{vw}	23 mΩ	X_{wu}	45 mΩ
X_{uvw}	43 mΩ				

larger than the value obtained by numerical analysis. This is because the mutual inductances used in the analysis are lower than the measured mutual inductances. The transmitter coils form a hexagonal shape and have the dimensions as presented in Fig. 6. Because the mutual inductances M_{uv}, M_{vw}, and M_{wu} between the transmitter coils are negative, an inductor L_0 is employed as X_0. Since there are differences between the mutual inductances because of manufacturing error, an average of the inductances is used to set L_0. Similarly, the self-inductances of the transmitter coils differ from each other. The different resonant capacitances are set so that the reactance values become nearly zero for every transmitter coil. Table 3 lists the measured reactance values of the transmitter coils that have been compensated by the inductor and capacitors. For example, X_u stands for the reactance value of the coil L_u while the other coils are in an open circuit. Similarly, X_{uv} stands for the reactance value of the compensated coil L_u and coil L_v in parallel while the coil L_w is in open circuit. It is confirmed that the reactance values are significantly low in every case. For the command generation in the control, the resistance r_1 was set to the sum of the averaged coil resistance and a conductive resistance of 60 mΩ of the switches (MOSFET of ROHM, SCT3060) in the inverter. The receiver coil forms a circular shape, with an outer diameter of 200 mm and an inner diameter of 152 mm. The receiver coil is set with a vertical gap length, l_g of 50 mm.

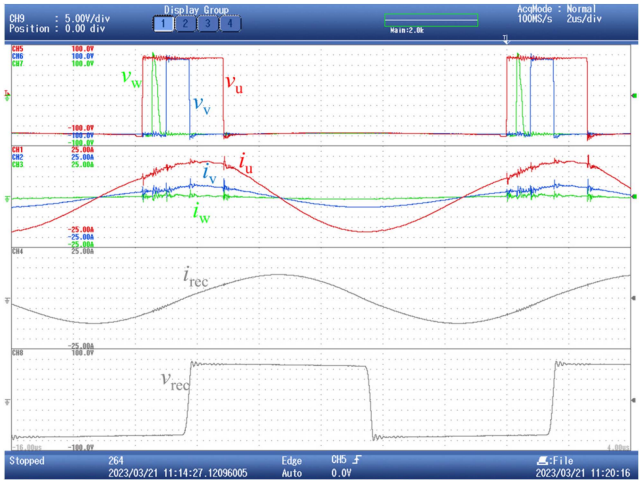

FIGURE 16. Waveforms in the steady state when the receiver coil is at P3.

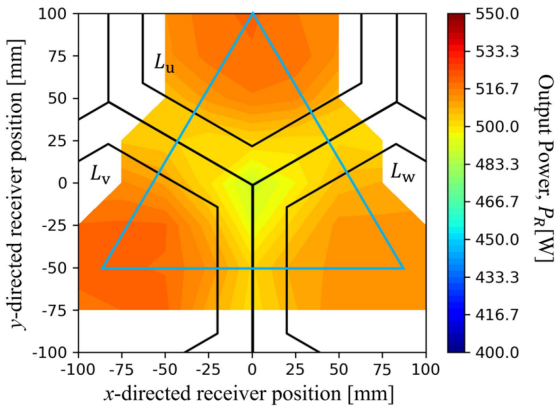

FIGURE 17. Measured output powers at receiver positions.

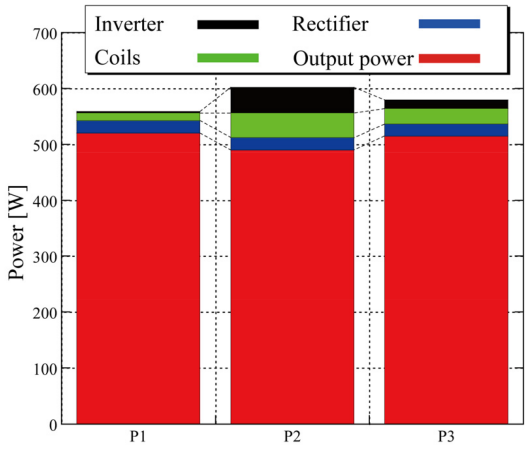

FIGURE 18. Breakdowns of the power and losses in the system.

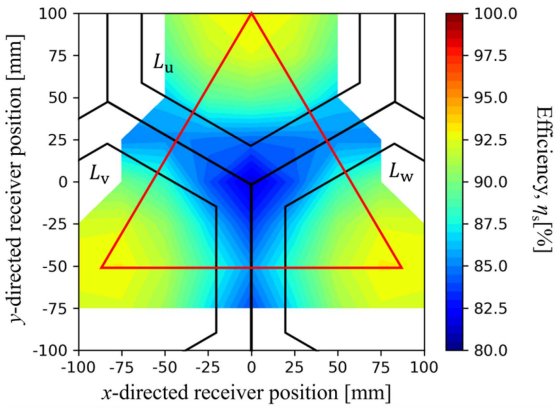

FIGURE 19. Measured efficiencies of the whole system at receiver positions.

B. EXPERIMENTAL RESULTS

Fig. 16 shows waveforms under the proposed control with a P_{2c} of 550 W. The receiver coil is set at P3, where the mutual inductances M_{u2}, M_{v2}, and M_{w2} are 9.45, 2.70, and 0.315 μH, respectively, in measurement. Because the resistances of the transmitter coils are uniform, the ratio of the optimal currents approximately corresponds with the ratio of these mutual inductances. The result confirms that the controller can adjust the currents in this manner. Although the current i_v is distorted, the receiver current varies sinusoidally. Thus, the harmonics in the currents through the transmitter coils do not influence the power transfer. This is why control deals with only the fundamentals of the currents.

Fig. 17 shows the output powers under the proposed control. The power command value is set at P_{2c}= 550 W. Inside the triangle, 520 W is measured as a peak power at the center of L_v, and 490 W is marked as a valley at P2. The variation is only 5.77%. Fig. 18 shows the breakdowns of the losses and output power in the system, which were obtained by the measurements. At P1, the transferred power P_2, which is the sum of the output power, the resistive loss of the receiver coil, and the loss of the rectifier, is approximately 550 W. Alternatively, at P2, the transferred power is 525 W, which is lower than $P_{2c} = 550$ W. This slight reduction is caused by the conduction loss in L_0, the switching loss in the MOSFET, and, especially, the deviation of the resonant circuit. The mutual inductance used for determining L_0 is an average value. The difference from the actual values generates a little reactance and causes the controller to fail in accurate estimation of the induced voltages V_{ui}, V_{vi}, and V_{wi}. These factors are reinforced at P2, because the sum of squared currents through L_0 is the largest.

Fig. 19 shows efficiencies η_s of the whole system at $P_{2c} = 550$ W. An efficiency of 93.13% is marked as a peak at the center of L_v and 81.42% is marked as a valley at P3. The lowest efficiency at P3 is caused by the largest losses in the inverter as well as the coils due to the largest currents, as shown in Fig. 18.

Fig. 20 shows efficiencies η_s at $P_R = 200$ W, without the proposed control, when the receiver is at P3. The current command calculated by (14) is close to the current combination with the maximum efficiency. The maximum efficiency is 87.40%. The efficiency at the command value is 86.72%, which is only 0.7% lower than the maximum efficiency. The

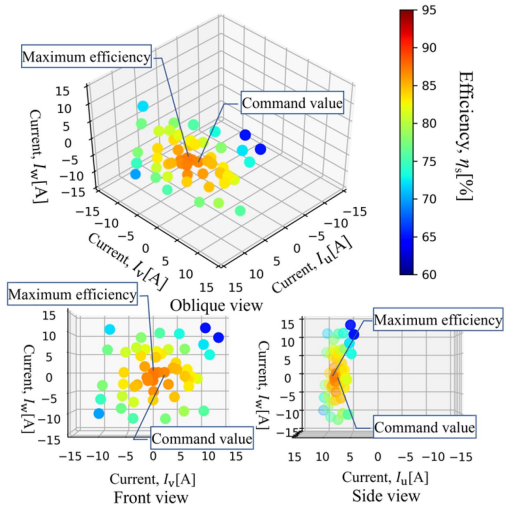

FIGURE 20. Measured efficiencies of the whole system when the receiver coil is at P3.

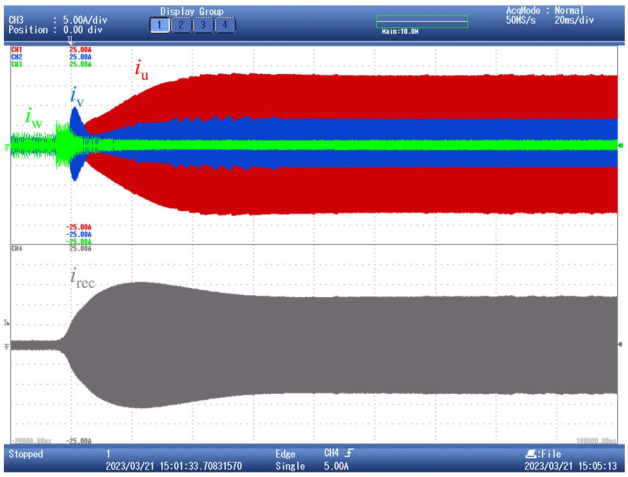

FIGURE 21. Waveforms in the transient state when the receiver coil is at P3.

deviation between the command and the optimal current is caused by the loss in the inverter.

Fig. 21 shows the waveforms in the transient state when the receiver is at P3. When the receiver coil is absent, the controller outputs currents with a low amplitude, which is needed for the controller to detect the proximity of the receiver coil. When the receiver coil approaches, the induced voltages V_{ui}, V_{vi}, and V_{wi} increase, and then the controller starts operating in accordance with the optimal current command. In this experiment, the inverter flows currents with an amplitude of 1.4 A ahead of the optimal current control. At 15 ms, the inverter begins the optimal current control. Then, the amplitudes of the currents gradually change and end up with the optimal current at 100 ms.

VII. CONCLUSION

This article proposed a circuit configuration for coil-array wireless power transmitters with regularly arranged coils with an angular interval of 120°. The system has a circuit configuration where the inductances of the coils, including the mutual inductances between the transmitter coils, can be canceled. The system controls the currents through the transmitter coils so that the efficiency between the transmitter coils and the receiver coil is maximized and the transferred power is uniform regardless of the receiver position. The experiments validate the effective performance of the system; the variation of the output power can be suppressed to less than 5.8%, and the efficiency of the whole system is approximately maximized. Theoretically, these effective performances are available regardless of the shape, dimensions, and number of turns of the transmitter coils. Future work should deal with the expanded coil array with more than three coils and reveal an effective switching method for the switch set between the inverter and the coils, in addition to an algorithm for receiver position detection.

REFERENCES

[1] F. Farajizadeh, D. M. Vilathgamuwa, D. Jovanovic, P. Jayathurathnage, G. Ledwich, and U. Madawala, "Expandable N-legged converter to drive closely spaced multitransmitter wireless power transfer systems for dynamic charging," *IEEE Trans. Power Electron.*, vol. 35, no. 4, pp. 3794–3806, Apr. 2020.

[2] H. Matsumoto, R. Noborikawa, T. Zaitsu, and Y. Shibako, "Wireless power transfer system with passive boost topology for AGVs," *IEEE Open J. Ind. Appl.*, vol. 1, pp. 227–235, Nov. 2020.

[3] X. Liu and S. Y. Hui, "Simulation study and experimental verification of a universal contactless battery charging platform with localized charging features," *IEEE Trans. Power Electron.*, vol. 22, no. 6, pp. 2202–2210, Nov. 2007.

[4] H. Matsumoto, Y. Neba, K. Ishizaka, and R. Itoh, "Comparison of characteristics on planar contactless power transfer systems," *IEEE Trans. Power Electron.*, vol. 27, no. 6, pp. 2980–2993, Jun. 2012.

[5] W. X. Zhong, X. Liu, and S. Y. R. Hui, "A novel single-layer winding array and receiver coil structure for contactless battery charging systems with free-positioning and localized charging features," *IEEE Trans. Ind. Electron.*, vol. 58, no. 9, pp. 4136–4144, Sep. 2011.

[6] Y. Zhang, S. Chen, X. Li, and Y. Tang, "Design methodology of free-positioning nonoverlapping wireless charging for consumer electronics based on antiparallel windings," *IEEE Trans. Ind. Electron.*, vol. 69, no. 1, pp. 825–834, Jan. 2022.

[7] X. Mou, O. Groling, and H. Sun, "Energy-efficient and adaptive design for wireless power transfer in electric vehicles," *IEEE Trans. Ind. Electron.*, vol. 64, no. 9, pp. 7250–7260, Sep. 2017.

[8] L. Chen, G. R. Nagendra, J. T. Boys, and G. A. Covic, "Double-coupled systems for IPT roadway applications," *IEEE J. Emerg. Sel. Topics Power Electron.*, vol. 3, no. 1, pp. 37–49, Mar. 2015.

[9] T. Fujita, T. Yasuda, and H. Akagi, "A dynamic wireless power transfer system applicable to a stationary system," *IEEE Trans. Ind. Appl.*, vol. 53, no. 4, pp. 3748–3757, Jul./Aug. 2017.

[10] S. Y. Jeong, J. H. Park, G. P. Hong, and C. T. Rim, " Autotuning control system by variation of self-inductance for dynamic wireless ev charging with small air gap," *IEEE Trans. Power Electron.*, vol. 34, no. 6, pp. 5165–5174, Jun. 2019.

[11] X. Li, J. Hu, H. Wang, X. Dai, and Y. Sun, "A new coupling structure and position detection method for segmented control dynamic wireless power transfer systems," *IEEE Trans. Power Electron.*, vol. 35, no. 7, pp. 6741–6745, Jul. 2020.

[12] T. Arakawa et al., "Optimizing wireless power transfer from multiple transmit coils," *IEEE Access*, vol. 6, pp. 23828–23838, Apr. 2018.

[13] S.-J. Jeon and D.-W. Seo, "Effect of additional transmitting coils on transfer distance in multiple-transmitter wireless power transfer system," *IEEE Access*, vol. 10, pp. 9174–9183, Jan. 2022.

[14] E. Chaidee, A. Sangswang, S. Naetiladdanon, and S. Nutwong, "An inverter topology for multi transmitter wireless power transfer systems," *IEEE Access*, vol. 10, pp. 36592–36605, Mar. 2022.

[15] S. A. A. Mahmud, I. Panhwar, and P. Jayathurathnage, "Large-area free-positioning wireless power transfer to movable receivers," *IEEE Trans. Ind. Electron.*, vol. 69, no. 12, pp. 12807–12816, Dec. 2022.
[16] X. Tian, K. T. Chau, Z. Hua, and W. Han, "Design and analysis of demand-customized selective wireless power transfer system," *IEEE Trans. Ind. Electron.*, vol. 69, no. 12, pp. 13451–13461, Dec. 2022.
[17] F. Farajizadeh, D. M. Vilathgamuwa, D. Jovanovic, P. Jayathurathnage, G. Ledwich, and U. Madawala, "Expandable N-legged converter to drive closely spaced multitransmitter wireless power transfer systems for dynamic charging," *IEEE Trans. Power Electron.*, vol. 35, no. 4, pp. 3794–3806, Apr. 2020.
[18] V. Z. Barsari, D. J. Thrimawithana, and G. A. Covic, "An inductive coupler array for in-motion wireless charging of electric vehicles," *EEE Trans. Power Electron.*, vol. 36, no. 9, pp. 9854–9863, Sep. 2021.
[19] P. Tan, T. Peng, X. Gao, and B. Zhang, "Flexible combination and switching control for robust wireless power transfer system with hexagonal array coil," *IEEE Trans. Power Electron.*, vol. 36, no. 4, pp. 3868–3882, Apr. 2021.
[20] B. Lee, D. Ahn, and M. Ghovanloo, "Three-phase time-multiplexed planar power transmission to distributed implants," *IEEE Emerg. Sel. Topics Power Electron.*, vol. 4, no. 1, pp. 263–272, Mar. 2016.
[21] C. Zhang, D. Lin, and S. Y. Hui, "Basic control principles of omnidirectional wireless power transfer," *IEEE Trans. Power Electron.*, vol. 31, no. 7, pp. 5215–5227, Jul. 2016.
[22] L. Tan et al., "Power stability optimization design of three-dimensional wireless power transmission system in multi-load application scenarios," *IEEE Access*, vol. 8, pp. 91843–91854, 2020.
[23] M. Pathmanathan, S. Nie, N. Yakop, and P. W. Lehn, "Field-oriented control of a three-phase wireless power transfer system transmitter," *IEEE Trans. Transp. Electrific.*, vol. 5, no. 4, pp. 1015–1026, Dec. 2019.
[24] H. Kanazawa, H. Uwai, S. Kiuchi, and H. Matsumoto, "Receiver-position-based unbalanced-current control for a three- to single-phase wireless power transfer system for AGVs," *IEEE Trans. Ind. Electron.*, vol. 70, no. 4, pp. 3245–3256, Apr. 2023.

HIROKAZU MATSUMOTO (Member, IEEE) was born in Ehime, Japan, in 1977. He received the M.S. degree in electrical and electronic systems engineering and the Dr.Eng. degree in engineering from Kyushu University, Fukuoka, Japan, in 2001 and 2004, respectively.

In 2004, he was a researcher of the 21st Century Center of Excellence Program. From 2005 to 2007, he was with Mitsubishi Electric Company, Japan, where he worked on the design of servo systems for factory automation. From 2008 to 2019, he was with the Department of Electrical Engineering, Fukuoka University. In 2017, he was a Visiting Professor with The Edward S. Rogers Sr. Department of Electrical & Computer Engineering, University of Toronto. Since 2019, he has been an Associate Professor with the Department of Electrical Engineering and Electronics, Aoyama Gakuin University, Kanagawa, Japan. His research interests include power inverters, wireless power transfer systems, electric motors, and their control.

WATARU YONEYAMA was born in Tokyo, Japan, in 1998. He received the B.S. degree in electrical and electronic engineering in 2021 from Aoyama Gakuin University, Kanagawa, Japan, where he is currently working toward the M.S. degree in electrical and electronic engineering with a thesis on wireless power transfer systems.

AOZORA HATA was born in Hyogo, Japan, in 1999. He received the B.S. degree in electrical and electronic engineering in 2022 from Aoyama Gakuin University, Kanagawa, Japan, where he is currently working toward the M.S. degree in electrical and electronic engineering with a thesis on wireless power transfer systems.

YUKI SATO (Member, IEEE) was born in Hokkaido, Japan, in 1989. He received the B.E. and M.E degrees in information science and the Ph.D. degree in engineering from Hokkaido University, Sapporo, Japan, in 2012, 2014, and 2017, respectively.

From 2017 to 2022, he was with Kilby Labs, Texas Instruments Japan Limited. He is currently an Assistant Professor with the Department of Electrical Engineering and Electronics, Aoyama Gakuin University, Kanagawa, Japan. His research interests include computational electromagnetism, design optimization, and the SPICE model for magnetic components.